J. Fluid Mech. (1991), *vol.* 228, *pp.* 443–463
Printed in Great Britain

On the stability of compressible flow past axisymmetric bodies

By M. R. MALIK AND R. E. SPALL
High Technology Corporation, P.O. Box 7262, Hampton, VA 23666, USA

(Received 19 October 1989)

Compressible linear stability theory for axisymmetric flows is presented. The theory is applied to flow past a cylinder and a sharp cone at a Mach number of 5 with adiabatic wall conditions. The effect of transverse curvature and body divergence is studied. It is found that transverse curvature has a stabilizing influence on axisymmetric (first and second mode) disturbances while it has a destabilizing influence on the asymmetric (oblique first mode) disturbances. The body divergence effects are stabilizing for both symmetric and asymmetric disturbances. Comparisons made with the results of planar stability theory show that, for a cylinder, curvature effects become more pronounced with increasing distance along the cylinder. For a sharp cone, these effects become less significant further away from the cone tip since the body radius increases faster than the growth of the boundary layer. The effect of cone angle on stability is also studied.

1. Introduction

Recent theoretical and experimental studies (e.g. Malik 1989*a*; Chen, Malik & Beckwith 1989) have shown that compressible linear stability (Lees & Lin 1946; Mack 1969) can be used as a guide for estimation of the location of transition in supersonic boundary layers when transition takes place in low-disturbance environments, and in the absence of any 'bypass' mechanisms (Morkovin 1969). Therefore, the subject of compressible linear stability is not only of fundamental interest in fluid mechanics, it is also relevant in the design of many aerodynamic configurations at supersonic and hypersonic speeds.

The stability of the compressible flat-plate boundary layer has been studied by many authors (see e.g. Lees & Reshotko 1962; Mack 1969, 1984; Gapanov 1981). There are two important modes of instability present in a compressible flat-plate boundary layer. The first mode is an extension to high speeds of the Tollmien–Schlichting (TS) instability present in incompressible flows, though for supersonic Mach numbers it differs in one aspect in that it is most amplified when oblique. This mode represents viscous instability at low Mach numbers, but the inviscid nature of the instability begins to dominate when Mach number increases since compressible flat-plate boundary-layer profiles contain a generalized inflexion point (i.e. $\mathrm{d}/\mathrm{d}y(\rho\,\mathrm{d}u/\mathrm{d}y) = 0$ at some point in the boundary layer). This mode may be stabilized by wall cooling, suction and favourable pressure gradient. The second mode is the result of an inviscid instability which is present owing to a region of supersonic mean flow relative to the disturbance phase velocity. In fact, when this supersonic relative flow is present, there exist an infinite number of modes in the boundary layer. However, the first mode belonging to this family, commonly known

as Mack's second mode, is most relevant, since it is known to have the highest growth rate. The second mode becomes important at Mach numbers above about 4 and has growth rates much higher than the first mode. The existence of both the first and second modes was established by the experiments of Kendall (1975), Demetriades (1974) and Stetson *et al.* (1983). The second mode is different in character with respect to the first mode; it is most amplified when two-dimensional and is destabilized with wall cooling (Mack 1969). It was found by Malik (1989*a*) that this mode can be stabilized with wall suction and a favourable pressure gradient.

Since axisymmetric bodies represent many practical configurations, it is important to study the stability of such flows. In particular, it is of interest to investigate the effect of transverse curvature and body divergence on boundary-layer stability. The profound effect that curvature (of body and wavefront) can have on the stability of three-dimensional incompressible flow was clearly demonstrated by Malik, Wilkinson & Orszag (1981) and Malik & Poll (1985). Malik (1984), Mack (1987) and Gasperas (1987) used linear theory to investigate the compressible stability of supersonic flow past sharp cones, but they all ignored transverse curvature effects. Gasperas included the body divergence effect on the stability analysis and found the effect to be stabilizing. However, he only studied the axisymmetric second-mode disturbances. Recently, Duck (1990) and Duck & Hall (1989) have studied the inviscid and viscous instability of supersonic flow along a cylinder using asymptotic methods. Their work on the viscous instability follows from that of Smith (1989) for a flat plate.

Chen *et al.* (1989) included both the transverse curvature and body divergence effects in their calculations for Mach 3.5 flow past a sharp cone; however, no theoretical details were given. The main purpose of their paper was to present experimental results on transition in a flat-plate and sharp-cone boundary layer performed in a Mach 3.5 low-disturbance tunnel (Beckwith *et al.* 1983). Their experimental results showed that the transition Reynolds number on the flat plate was higher than on a cone, which is also what the stability theory calculations indicated. The experiment of Chen *et al.* (1989) thus resolved a longstanding controversy regarding transition on flat plates and cones. Earlier, Pate (1971) had presented a correlation of transition data for flat plates and cones which indicated that the ratio of sharp-cone to flat-plate transition Reynolds number was greater than unity, and in particular at Mach 3.5 the ratio was about 2.2. The experiments correlated by Pate (1971) were performed in conventional supersonic wind tunnels which have turbulent boundary layers on the nozzle walls which radiate noise and thus significantly influence the transition Reynolds number, particularly on the flat plate. The experiment of Chen *et al.* (1989) showed that the trend of $(Re_t)_{\text{cone}}/(Re_t)_{\text{flat plate}}$ is altered when the experiment is performed in the low-disturbance tunnel. In this experiment, the ratio was 0.8 (as compared to 2.2 in Pate's 1971 work) which is in reasonable agreement with the results of linear stability theory. The adverse effect that wind tunnel noise can have on transition Reynolds number was earlier demonstrated by the work of Pate & Scheuler (1969). It appears that this effect is much stronger for the flat plate than on the sharp cone. In any case, when high noise levels are present the relevance of linear stability theory to the transition process is, at best, dubious. However, in low-disturbance environments, such as in flight, and in the absence of 'bypass' transition (Morkovin 1969) the results of linear theory are of some practical significance.

In this paper, we present viscous, compressible linear stability equations for an axisymmetric basic flow. Both axisymmetric and non-axisymmetric disturbances are considered. The theory is applicable to axisymmetric bodies of arbitrary shape,

including blunt bodies and walls with concave curvature, and thus both the TS and Görtler instabilities may be investigated. However, in this study we consider bodies with sharp leading edges and compute the basic flow using boundary-layer theory. The non-similar form of the boundary-layer equations is solved by a marching finite-difference method. Linear stability results are then obtained for Mach 5 flow past a hollow cylinder and a sharp cone, and the effect of transverse curvature on both the first- and second-mode instability is studied. The effect of body divergence is investigated by studying the stability of sharp-cone boundary layers with various cone angles. In hypersonic flows, the shock wave provides an additional boundary condition for the stability problem, as discussed by Petrov (1985) and Cowley & Hall (1990). However, the shock wave effect is ignored in this study and is the subject of another paper (see Chang, Malik & Hussaini 1990).

2. Problem formulation

The equations governing the flow of a viscous compressible ideal gas are

$$\rho\left[\frac{\partial \boldsymbol{u}}{\partial t}+(\boldsymbol{u}\cdot\boldsymbol{\nabla})\,\boldsymbol{u}\right]=-\boldsymbol{\nabla}p+\boldsymbol{\nabla}\cdot[\lambda(\boldsymbol{\nabla}\cdot\boldsymbol{u})\boldsymbol{I}]+\boldsymbol{\nabla}\cdot[\mu(\boldsymbol{\nabla}\boldsymbol{u}+\boldsymbol{\nabla}\boldsymbol{u}^{\mathrm{tr}})], \tag{2.1}$$

$$\frac{\partial \rho}{\partial t}+\boldsymbol{\nabla}\cdot(\rho\boldsymbol{u})=0, \tag{2.2}$$

$$\rho c_p\left[\frac{\partial T}{\partial t}+(\boldsymbol{u}\cdot\boldsymbol{\nabla})\,T\right]=\boldsymbol{\nabla}\cdot(k\boldsymbol{\nabla}T)+\frac{\partial p}{\partial t}+(\boldsymbol{u}\cdot\boldsymbol{\nabla})\,p+\Phi, \tag{2.3}$$

$$p=\rho\mathfrak{R}T, \tag{2.4}$$

where $\boldsymbol{u}=(u,v,w)$ is the velocity vector, ρ the density, p the pressure, T the temperature, $\mathfrak{R}$ the gas constant, c_p the specific heat, k the thermal conductivity, μ the first coefficient of viscosity and λ the second coefficient of viscosity. The viscous dissipation Φ is given as

$$\Phi=\lambda(\boldsymbol{\nabla}\cdot\boldsymbol{u})^2+\tfrac{1}{2}\mu[\boldsymbol{\nabla}\boldsymbol{u}+\boldsymbol{\nabla}\boldsymbol{u}^{\mathrm{tr}}]^2. \tag{2.5}$$

We assume that the instantaneous flow field may be decomposed into a mean and a fluctuating part. For example, temperature T may be written as

$$T=\bar{T}+\tilde{T}, \tag{2.6}$$

where $\bar{T}$ represents the temperature of steady basic flow and $\tilde{T}$ is a time-dependent perturbation.

The governing equations for the steady, basic flow may be derived by invoking the boundary-layer assumption. Though real gas effects become important at hypersonic speeds in atmospheric flight, we consider air to be a perfect gas in this study. Real gas effects may be accounted for in a manner discussed by Malik (1989*b*).

2.1. *Boundary-layer flow*

We consider compressible flow past an axisymmetric body of radius $r_0(x)$, where x is the coordinate along the body while y is normal to it. The body is assumed to be at zero angle of attack. Depending upon the value of $r_0(x)$, the body may take the form of a cylinder, a sharp cone, a blunt cone, or in the limit of $r_0\to\infty$, a flate plate.

If $\bar{u}$ and $\bar{v}$ represent the velocity components along the x- and y-directions

respectively, then the boundary-layer equations in the presence of a pressure gradient are

$$\bar{\rho}\bar{u}\frac{\partial \bar{u}}{\partial x}+\bar{\rho}\bar{v}\frac{\partial \bar{u}}{\partial y}=-\frac{\mathrm{d}\bar{p}}{\mathrm{d}x}+\frac{1}{r^j}\frac{\partial}{\partial y}\left[r^j\bar{\mu}\frac{\partial \bar{u}}{\partial y}\right], \tag{2.7}$$

$$\frac{\partial}{\partial x}(r^j\bar{\rho}\bar{u})+\frac{\partial}{\partial y}(r^j\bar{\rho}\bar{v})=0, \tag{2.8}$$

$$\bar{\rho}\bar{c}_p\,\bar{u}\frac{\partial \bar{T}}{\partial x}+\bar{\rho}\bar{c}_p\,\bar{v}\frac{\partial \bar{T}}{\partial y}=\frac{1}{r^j}\frac{\partial}{\partial y}\left(r^j\bar{k}\frac{\partial \bar{T}}{\partial y}\right)+\bar{\mu}\left(\frac{\partial \bar{u}}{\partial y}\right)^2+\bar{u}\frac{\mathrm{d}\bar{p}}{\mathrm{d}x}, \tag{2.9}$$

where $j=0$ and $j=1$ represent two-dimensional and axisymmetric flows respectively. We note that r is related to r_0 according to

$$r(x,y)=r_0(x)+y\cos\lambda, \tag{2.10}$$

where the local value of angle λ signifies the slope of the body. For a cylinder, $\lambda=0$ and for a sharp cone λ is the cone half-angle.

The boundary-layer equations (2.7)–(2.9) are singular at $x=0$. In order to remove the singularity, we use Mangler–Levy–Lees transformation (see Probstein & Elliot 1956; Hayes & Probstein 1959):

$$\mathrm{d}\xi=\rho_e\mu_e u_e r_0^{2j}\,\mathrm{d}x, \tag{2.11a}$$

$$\mathrm{d}\eta=[u_e/(2\xi)^{\frac{1}{2}}]r^j\bar{\rho}\,\mathrm{d}y \tag{2.11b}$$

where the subscript e represents the value of variables at the edge of the boundary layer. If we define three parameters F, V, θ so that

$$F=\bar{u}/u_e \tag{2.12a}$$

$$V=\frac{2\xi}{\rho_e\mu_e u_e r_0^{2j}}\left[F\left(\frac{\partial\eta}{\partial x}\right)+\frac{\bar{\rho}\bar{v}r^j}{(2\xi)^{\frac{1}{2}}}\right] \tag{2.12b}$$

$$\theta=\bar{T}/T_e \tag{2.12c}$$

then the governing equations in the transformed (ξ,η)-space can be represented as

$$\frac{\partial}{\partial\eta}\left(a_1\frac{\partial F}{\partial\eta}\right)-V\frac{\partial F}{\partial\eta}+a_2(\theta-F^2)=2\xi F\frac{\partial F}{\partial\xi}, \tag{2.13}$$

$$\frac{\partial V}{\partial\eta}+F=2\xi\frac{\partial F}{\partial\xi}, \tag{2.14}$$

$$\frac{\partial}{\partial\eta}\left(a_3\frac{\partial\theta}{\partial\eta}\right)-V\frac{\partial\theta}{\partial\eta}+a_4\left(\frac{\partial F}{\partial\eta}\right)^2=2\xi F\frac{\partial\theta}{\partial\xi}, \tag{2.15}$$

where $$a_1=(1+\chi)^{2j}\frac{\bar{\rho}\bar{\mu}}{\rho_e\mu_e},\quad a_2=\frac{2\xi}{u_e}\frac{\mathrm{d}u_e}{\mathrm{d}\xi},\quad a_3=\frac{a_1}{\sigma},\quad a_4=(\gamma-1)M_e^2a_1, \tag{2.16a–d}$$

and χ is the transverse curvature parameter

$$\chi=y\cos\lambda/r_0 \tag{2.16e}$$

while γ is the ratio of specific heats and M_e and σ represent respectively the Mach number and the Prandtl number defined as

$$M_e=u_e/(\gamma\Re T_e)^{\frac{1}{2}}, \tag{2.17}$$

$$\sigma=\bar{\mu}\bar{c}_p/\bar{k}. \tag{2.18}$$

In deriving (2.15), it has been assumed that the specific heat $\bar{c}_p$ is constant. So, the air is considered to be a thermally and calorically perfect gas. The viscosity $\bar{\mu}$ is assumed to be given by the composite relation (as used by Mack 1984)

$$\bar{\mu} = 2.27 \times 10^{-8} \frac{\bar{T}^{\frac{1}{2}}}{1 + 198.6/\bar{T}} \text{ lb s/ft}^2; \quad \bar{T} \geqslant 198.6 \text{ °R}, \tag{2.19a}$$

$$\bar{\mu} = 8.0539 \times 10^{-10} \bar{T} \text{ lb s/ft}^2; \quad \bar{T} < 198.6 \text{ °R}. \tag{2.19b}$$

The thermal conductivity $\bar{k}$ may also be prescribed by a similar formula. For the results presented in this paper, however, we compute it by assuming a constant Prandtl number of 0.7. The effect of variable specific heat and Prandtl number has been discussed by Malik (1989*b*).

The advantage of using Mangler–Levy–Lees transformation, in addition to removing the singularity at $x = 0$, is that the boundary-layer thickness remains finite in the transformed coordinate η. The solution of the non-similar boundary-layer equations (2.13)–(2.15) is obtained by the second-order finite-difference method of Harris & Blanchard (1982) and the resulting profiles are used in the stability analysis.

For a sharp cone, if transverse curvature is neglected ($\chi = 0$), then (2.13)–(2.15) simplify to the following similarity equations:

$$\frac{\partial}{\partial \eta}\left(a_1 \frac{\partial F}{\partial \eta}\right) - V \frac{\partial F}{\partial \eta}, \tag{2.20}$$

$$\frac{\partial V}{\partial \eta} + F = 0, \tag{2.21}$$

$$\frac{\partial}{\partial \eta}\left(a_3 \frac{\partial \theta}{\partial \eta}\right) - V \frac{\partial \theta}{\partial \eta} + a_4 \left(\frac{\partial F}{\partial \eta}\right)^2 = 0, \tag{2.22}$$

which are also the governing equations for the boundary-layer flow past a flat plate. Since for a sharp cone $r_0 = x \sin \lambda$, (2.11*a*) reduces to

$$\mathrm{d}\xi = \rho_e \mu_e u_e (x \sin \lambda)^2 \, \mathrm{d}x \tag{2.23a}$$

which yields

$$\xi = \tfrac{1}{3} \rho_e \mu_e u_e \sin^2 \lambda x^3. \tag{2.23b}$$

Thus, (2.11*b*) can be written as

$$\mathrm{d}\eta = \frac{u_e x \sin \lambda}{(\frac{2}{3} \rho_e \mu_e u_e x^3 \sin^2 \lambda)^{\frac{1}{2}}} \rho \, \mathrm{d}y \tag{2.23c}$$

or

$$\mathrm{d}y = \left(\frac{2\nu_e x}{3u_e}\right)^{\frac{1}{2}} \frac{\rho_e}{\rho} \mathrm{d}\eta. \tag{2.23d}$$

In other words, for identical edge conditions the cone mean flow profiles at a location x_c can be obtained from flat-plate profiles at another location x_t if $x_c = 3x_t$. This is the main result of Mangler–Stepanov transformation (see Stewartson 1964) and was used by Mack (1987) and Gasperas (1987) for computing the basic flow for sharp-cone boundary layers. We note that if transverse curvature is neglected for a cylinder, then the computed profiles along the cylinder are the same as for a flat plate. Equation (2.23*d*) also indicates that the cone boundary layer will be $\sqrt{3}$ times thinner than the flat-plate boundary layer at the same x-location. This implies that, relative to that of the flat plate, the sharp-cone boundary layer would support higher disturbance frequencies. In the present study, we solve (2.13)–(2.15) and do not

neglect the transverse curvature effect for the basic flow. However, we will also comment on the effect of neglecting curvature in the mean flow by solving (2.20)–(2.22).

2.2. *Linear stability equations*

In order to derive the stability equations, we non-dimensionalize the governing equations by using some constant reference values for density, temperature, velocity, viscosity, thermal conductivity, and specific heat. We denote these scales to be ρ_e, T_e, u_e, μ_e, k_e and c_{p_e}. Pressure is scaled with $\rho_e u_e^2$ while the lengthscale is taken to be some reference length l. The non-dimensional form of the governing equations may be written as

$$\rho\left[\frac{\partial \boldsymbol{u}}{\partial t}+(\boldsymbol{u}\cdot\boldsymbol{\nabla})\,\boldsymbol{u}\right]=-\boldsymbol{\nabla}p+\frac{1}{R}\boldsymbol{\nabla}\cdot[\lambda(\boldsymbol{\nabla}\cdot\boldsymbol{u})\boldsymbol{I}]+\frac{1}{R}\boldsymbol{\nabla}\cdot[\mu(\boldsymbol{\nabla}\boldsymbol{u}+\boldsymbol{\nabla}\boldsymbol{u}^{\mathrm{tr}})], \tag{2.24}$$

$$\frac{\partial \rho}{\partial t}+\boldsymbol{\nabla}\cdot\rho\boldsymbol{u}=0, \tag{2.25}$$

$$\rho c_p\left[\frac{\partial T}{\partial t}+(\boldsymbol{u}\cdot\boldsymbol{\nabla})\,T\right]-(\gamma-1)M_e^2\left[\frac{\partial p}{\partial t}+(\boldsymbol{u}\cdot\boldsymbol{\nabla})\,p\right]=\frac{1}{RPr}[k\nabla^2 T+\boldsymbol{\nabla}k\cdot\boldsymbol{\nabla}T]+\frac{(\gamma-1)m_e^2}{R}\Phi, \tag{2.26}$$

$$\gamma M_e^2 p=\rho T, \tag{2.27}$$

where all the variables have been made non-dimensional with their respective scales. Other coefficients appearing in (2.24)–(2.27) are the Reynolds number R, and the Prandtl number Pr, which are defined as

$$R=\rho_e u_e \ell/\mu_e \tag{2.28}$$

$$Pr=\mu_e c_{p_e}/k_e. \tag{2.29}$$

The linear stability equations can now be derived by decomposing the flow field into a mean and a fluctuation part as in (2.6). Thus we obtain

$$\bar{\rho}\left[\frac{\partial \tilde{\boldsymbol{u}}}{\partial t}+\bar{\boldsymbol{u}}\cdot\boldsymbol{\nabla}\tilde{\boldsymbol{u}}+\tilde{\boldsymbol{u}}\cdot\boldsymbol{\nabla}\bar{\boldsymbol{u}}\right]+\tilde{\rho}\bar{\boldsymbol{u}}\cdot\boldsymbol{\nabla}\bar{\boldsymbol{u}}=-\boldsymbol{\nabla}\tilde{p}+\frac{1}{R}\boldsymbol{\nabla}\cdot[\bar{\lambda}(\boldsymbol{\nabla}\cdot\tilde{\boldsymbol{u}})\boldsymbol{I}+\tilde{\lambda}(\boldsymbol{\nabla}\cdot\bar{\boldsymbol{u}})\boldsymbol{I}]$$

$$+\frac{1}{R}\boldsymbol{\nabla}\cdot[\bar{\mu}(\boldsymbol{\nabla}\tilde{\boldsymbol{u}}+\boldsymbol{\nabla}\tilde{\boldsymbol{u}}^{\mathrm{tr}})+\tilde{\mu}(\boldsymbol{\nabla}\bar{\boldsymbol{u}}+\boldsymbol{\nabla}\bar{\boldsymbol{u}}^{\mathrm{tr}})], \tag{2.30}$$

$$\frac{\partial \tilde{\rho}}{\partial t}+\boldsymbol{\nabla}\cdot\bar{\rho}\tilde{\boldsymbol{u}}+\boldsymbol{\nabla}\cdot\tilde{\rho}\bar{\boldsymbol{u}}=0, \tag{2.31}$$

$$\bar{\rho}\bar{c}_p\left[\frac{\partial \tilde{T}}{\partial t}+\bar{\boldsymbol{u}}\cdot\boldsymbol{\nabla}\tilde{T}+\tilde{\boldsymbol{u}}\cdot\boldsymbol{\nabla}\bar{T}\right]+\tilde{\rho}\bar{c}_p\,\bar{\boldsymbol{u}}\cdot\boldsymbol{\nabla}\bar{T}+\bar{\rho}\tilde{c}_p\,\bar{\boldsymbol{u}}\cdot\boldsymbol{\nabla}\bar{T}=\frac{1}{RPr}[(\bar{k}\nabla^2\tilde{T}+\tilde{k}\nabla^2\bar{T})$$

$$+(\boldsymbol{\nabla}\bar{k}\cdot\boldsymbol{\nabla}\tilde{T}+\boldsymbol{\nabla}\tilde{k}\cdot\boldsymbol{\nabla}\bar{T})]+(\gamma-1)M_e^2\left[\frac{\partial \tilde{p}}{\partial t}+\bar{\boldsymbol{u}}\cdot\boldsymbol{\nabla}\tilde{p}+\tilde{\boldsymbol{u}}\cdot\boldsymbol{\nabla}\bar{p}\right]$$

$$+\frac{(\gamma-1)M_e^2}{R}\{2\bar{\lambda}(\boldsymbol{\nabla}\cdot\bar{\boldsymbol{u}})(\boldsymbol{\nabla}\cdot\tilde{\boldsymbol{u}})+\tilde{\lambda}(\boldsymbol{\nabla}\cdot\bar{\boldsymbol{u}})^2+\bar{\mu}[(\boldsymbol{\nabla}\bar{\boldsymbol{u}}+\boldsymbol{\nabla}\bar{\boldsymbol{u}}^{\mathrm{tr}}):(\boldsymbol{\nabla}\tilde{\boldsymbol{u}}+\boldsymbol{\nabla}\tilde{\boldsymbol{u}}^{\mathrm{tr}})]$$

$$+\tfrac{1}{2}\tilde{\mu}[(\boldsymbol{\nabla}\bar{\boldsymbol{u}}+\boldsymbol{\nabla}\bar{\boldsymbol{u}}^{\mathrm{tr}}):(\boldsymbol{\nabla}\bar{\boldsymbol{u}}+\boldsymbol{\nabla}\bar{\boldsymbol{u}}^{\mathrm{tr}})]\}, \tag{2.32}$$

$$\tilde{\rho}=\frac{\gamma M_e^2\tilde{p}}{\bar{T}}-\frac{\tilde{T}}{\bar{T}^2}, \tag{2.33}$$

where for a boundary layer $\bar{\rho}=1/\bar{T}$.

Let us restrict ourselves to flow past two-dimensional or axisymmetric bodies at zero incidence. We use body-fitted orthogonal curvilinear coordinates x, y, z, where x is the streamwise coordinate along the body surface, y is the coordinate normal to the surface and z is in the azimuthal direction. Elements of length in this system are $h_1\,\mathrm{d}x$, $\mathrm{d}y$ and $h_2\,\mathrm{d}z$. Therefore a general element of length is

$$\mathrm{d}s = [(h_1\,\mathrm{d}x)^2 + (\mathrm{d}y)^2 + (h_2\,\mathrm{d}z)^2]^{\frac{1}{2}},$$

and the velocity components in the x-, y- and z-directions are u, v and w respectively.

We consider the stability of quasi-parallel compressible flow. The 'quasi-parallel flow' assumption is the same as used in the Orr–Sommerfeld analysis of the incompressible boundary-layer flow (Tollmien 1929). Under this assumption,

$$\bar{u} = \bar{U}(y); \quad \bar{v} = 0; \quad \bar{T} = \bar{T}(y); \quad \bar{P} = \bar{P}(y); \quad \bar{\rho} = \bar{\rho}(y) \tag{2.34a}$$

and

$$\bar{w} = 0 \tag{2.34b}$$

because of the two-dimensional or axisymmetric nature of the basic flow. A number of terms drop out in (2.30)–(2.33) owing to these assumptions.

There is no *a priori* justification for the parallel-flow approximation except at high Reynolds numbers where, depending upon the disturbance characteristics, it may be formally valid. At finite Reynolds numbers, the parallel-flow approximation introduces an unknown amount of error in the solution. For incompressible Blasius flow, Gaster (1974) found that non-parallel effects are small. However, Smith (1989) found that for supersonic flows, parallel-flow approximation is very restrictive for TS waves, i.e. $M_e \ll R^{\frac{1}{5}}$ for the approximation to be valid. For low supersonic Mach numbers this inequality can be satisfied at Reynolds numbers of interest. On the other hand, this criterion is violated at higher Mach numbers for finite Reynolds numbers of practical interest. However, it may be argued that at these high Mach numbers, the dominant instability is inviscid (both the first and second mode) and not the lower branch triple-deck TS type considered by Smith. Non-parallel multiple-scale calculations of Gapanov (1981) and El-Hady (1981) for Mach 4.5 flat-plate flow showed the effect of boundary-layer growth to be small. At this Mach number, the results of the quasi-parallel and multiple-scale non-parallel stability theories are in fair agreement with the experiment of Kendall (1975), both for the first and second modes. Therefore, the qualitative nature of the influence of curvature on boundary-layer stability can be investigated by using the quasi-parallel theory. However, it will be important to study the combined effects of curvature and non-parallel flow, and we intend to do that in a future paper.

When the basic flow is parallel, one can assume that the disturbance quantities are given by a harmonic wave of the form

$$\tilde{T}(x, y, z, t) = \hat{T}(y)\,\mathrm{e}^{\mathrm{i}(\alpha x + \beta z - \omega t)}, \tag{2.35a}$$

where α and β are the wavenumbers and ω is the disturbance frequency. For an axisymmetric body of radius r_0,

$$\beta = n\ell/r_0, \tag{2.35b}$$

where n is the mode number for asymmetric disturbances. Substituting (2.34)–(2.35) into the linearized equations of motion and state (2.30)–(2.31), and dropping bars from the mean flow quantities, we obtain the following system of equations:

$$\frac{\mathrm{d}^2\hat{u}}{\mathrm{d}y^2}+(c_1T'+m_{13}+m_{23})\frac{\mathrm{d}\hat{u}}{\mathrm{d}y}+\mathrm{i}\alpha_0 l_1\frac{\mathrm{d}\hat{v}}{\mathrm{d}y}+c_1(U'-Um_{13})\frac{\mathrm{d}\hat{T}}{\mathrm{d}y}$$
$$+\left[\frac{\mathrm{i}c_3R}{\mu T}-l_2\alpha_0^2-\beta_0^2+\mathrm{i}\alpha_0 l_2 m_{21}-c_1T'm_{13}-l_2m_{21}^2-m_{13}m_{23}-m_{13}^2\right]\hat{u}$$
$$+\left[\mathrm{i}\alpha_0(c_1T'+l_1m_{23}+l_3m_{13})-\frac{R(U'+Um_{13})}{\mu T}+m_{21}(2m_{13}-l_2m_{21})\right]\hat{v}-\frac{\mathrm{i}\alpha_0R\hat{p}}{\mu}$$
$$+[c_1\{U''+(m_{13}+m_{23})U'+\mathrm{i}\alpha_0 l_0Um_{21}-l_2Um_{21}^2-Um_{13}(m_{13}+m_{23})\}$$
$$+c_2(U'-Um_{13})T']\hat{T}-[\alpha_0\beta_0l_1+\mathrm{i}\beta_0l_3m_{21}]\hat{w}=0, \tag{2.36}$$

$$\frac{\mathrm{d}^2\hat{v}}{\mathrm{d}y^2}+\frac{(\mathrm{i}\alpha_0+m_{21})l_1}{l_2}\frac{\mathrm{d}\hat{u}}{\mathrm{d}y}+(c_1T'+m_{13}+m_{23})\frac{\mathrm{d}\hat{v}}{\mathrm{d}y}-\frac{R}{l_2\mu}\frac{\mathrm{d}\hat{p}}{\mathrm{d}y}+\frac{c_1Um_{21}l_0}{l_2}\frac{\mathrm{d}\hat{T}}{\mathrm{d}y}$$
$$+\frac{\mathrm{i}\beta_0l_1}{l_2}\frac{\mathrm{d}\hat{w}}{\mathrm{d}y}+\left[\frac{1}{l_2}\left\{c_1T'(\mathrm{i}\alpha_0+m_{21})l_0+\frac{2RUm_{13}}{\mu T}-\mathrm{i}\alpha_0m_{13}l_3-m_{13}m_{21}l_1\right\}-m_{21}m_{23}\right]\hat{u}$$
$$+\left[\frac{1}{l_2}\{\mathrm{i}c_3R/\mu T-\alpha_0^2-\beta_0^2+\mathrm{i}\alpha_0m_{21}+c_1T'(m_{13}+m_{23})l_0\}-(m_{13}^2+m_{23}^2)\right]\hat{v}$$
$$+\left[\frac{\gamma M_e^2RU^2m_{13}}{\mu Tl_2}\right]\hat{p}+\left[\left\{\mathrm{i}\alpha_0c_1U'-\frac{RU^2m_{13}}{\mu T^2}+c_1(U'm_{21}l_1-Um_{21}m_{23}-Um_{13}m_{21}l_1\right.\right.$$
$$\left.\left.-\mathrm{i}\alpha_0Um_{13})+c_2UT'm_{21}l_0\right\}\frac{1}{l_2}-c_1Um_{21}m_{23}\right]\hat{T}+\left[\frac{\mathrm{i}\beta_0(c_1T'l_0-m_{23}l_3)}{l_2}\right]\hat{w}=0, \tag{2.37}$$

$$\frac{\mathrm{d}\hat{v}}{\mathrm{d}y}+(\mathrm{i}\alpha_0+m_{21})\hat{u}+\left[m_{13}+m_{23}-\frac{T'}{T}\right]\hat{v}+\gamma M_e^2(m_{21}U-\mathrm{i}c_3)\hat{p}-\left[\frac{m_{21}U-\mathrm{i}c_3}{T}\right]\hat{T}+\mathrm{i}\beta_0\hat{w}=0, \tag{2.38}$$

$$\frac{\mathrm{d}^2\hat{T}}{\mathrm{d}y^2}+c_4(U'-Um_{13})\frac{\mathrm{d}\hat{u}}{\mathrm{d}y}+(c_4Um_{21}l_0)\frac{\mathrm{d}\hat{v}}{\mathrm{d}y}+\left(\frac{2k'}{k}+m_{13}+m_{23}\right)\frac{\mathrm{d}\hat{T}}{\mathrm{d}y}+c_4[\mathrm{i}\alpha_0Um_{21}l_0-U'm_{13}$$
$$+Um_{21}^2l_2+Um_{13}^2]\hat{u}+\left[c_4\{\mathrm{i}\alpha_0(U'-Um_{13})+Um_{21}(m_{13}l_0+m_{23}l_2)\}-\frac{\sigma RT'}{\mu T}\right]\hat{v}-\left[\frac{\mathrm{i}c_3c_4R}{2\mu}\right]\hat{p}$$
$$+\left[\frac{\mathrm{i}c_3R\sigma}{\mu T}-a_0^2-\beta_0^2+\mathrm{i}\alpha_0m_{21}+c_1c_4\{\tfrac{1}{2}(U'^2+U^2(m_{21}^2l_2\right.$$
$$\left.+m_{13}^2))-UU'm_{13}\}+\frac{(m_{13}+m_{23})k'}{k}+\frac{k''}{k}\right]\hat{T}+(\mathrm{i}\beta_0c_4Um_{21}l_2)\hat{w}=0, \tag{2.39}$$

$$\frac{\mathrm{d}^2\hat{w}}{\mathrm{d}y^2}+\mathrm{i}\beta_0l_1\frac{\mathrm{d}\hat{v}}{\mathrm{d}y}+(c_1T'+m_{13}+m_{23})\frac{\mathrm{d}\hat{w}}{\mathrm{d}y}+(\mathrm{i}\beta_0m_{21}l_3-\alpha_0\beta_0l_1)\hat{u}+\mathrm{i}\beta_0(c_1T'+l_1m_{13}$$
$$+l_3m_{23})\hat{v}-\left(\frac{\mathrm{i}\beta_0R}{\mu}\right)\hat{p}+(\mathrm{i}\beta_0c_1Um_{21}l_2)\hat{T}+\left[\frac{(\mathrm{i}c_3-m_{21}U)R}{\mu T}-\alpha_0^2-l_2\beta_0^2+\mathrm{i}\alpha_0m_{21}-m_{21}^2\right.$$
$$\left.-m_{23}(c_1T'+m_{13}+m_{23})\right]\hat{w}=0, \tag{2.40}$$

where $(\,)'\equiv \mathrm{d}/\mathrm{d}y$, $l_q=q+\lambda/\mu$ and

$$c_1=\frac{1}{\mu}\frac{\mathrm{d}\mu}{\mathrm{d}T},\quad c_2=\frac{1}{\mu}\frac{\mathrm{d}^2\mu}{\mathrm{d}T^2},\quad c_3=-(\alpha U-\omega),\quad c_4=2(\gamma-1)M_e^2\sigma.$$

The curvature coefficients m_{13}, m_{21} and m_{23} are defined as

$$m_{13} = \frac{1}{h_1}\frac{\partial h_1}{\partial y}, \quad m_{21} = \frac{1}{h_1 h_2}\frac{\partial h_2}{\partial x}, \quad m_{23} = \frac{1}{h_2}\frac{\partial h_2}{\partial y},$$

and

$$\alpha_0 = \alpha/h_1, \quad \beta_0 = \beta/h_2.$$

In this study, since we only consider flow along a cylinder or a sharp cone, streamwise curvature is absent, i.e. $m_{13} = 0$ both for the cylinder and the sharp cone. Thus, only the parameters m_{21} and m_{23} need to be prescribed. Among these, m_{21} is related to body divergence due to increase in the body radius and m_{23} represents purely transverse curvature effect. However, these two effects are interrelated and cannot, in general, be separated as is evident from (2.42) below. Since the radius of a cylinder is constant, $m_{21} = 0$ while m_{23} can be written as

$$m_{23} = \epsilon/(1+\epsilon y), \tag{2.41a}$$

where

$$\epsilon = \ell/r_0. \tag{2.41b}$$

For a sharp cone of half-angle λ, both m_{21} and m_{23} are non-zero and are given as

$$m_{21} = \frac{\mathrm{d}(\ln r_0)/\mathrm{d}x}{1+\epsilon y} = \frac{\ell \sin\lambda}{r_0(1+\epsilon y)}, \tag{2.42a}$$

$$m_{23} = \frac{\epsilon}{1+\epsilon y}, \tag{2.42b}$$

where ϵ is given as

$$\epsilon = \ell \cos\lambda/r_0. \tag{2.42c}$$

Gasperas (1987), in his analysis of second-mode axisymmetric disturbances used $m_{23} = 0$ and set $m_{21} = \ell \sin\lambda/r_0$. We note that if all curvature coefficients are set to zero, the planar stability equations for a flat plate are recovered.

Equations (2.36)–(2.40) are to be solved subject to boundary conditions

$$\hat{u} = \hat{v} = \hat{w} = \hat{T} = 0; \quad y = 0, \tag{2.43}$$

$$\hat{u}, \hat{v}, \hat{w}, \hat{T} \to 0; \quad y \to \infty. \tag{2.44}$$

Equations (2.36)–(2.40) along with the homogeneous boundary conditions (2.43)–(2.44) constitute an eigenvalue problem described by the complex dispersion relation

$$\alpha = \alpha(\beta, \omega). \tag{2.45}$$

In the present study we consider spatial stability and assume β and ω to be real while α is complex. The imaginary part of α represents the disturbance growth rate ($-\alpha_i > 0$ implies instability).

2.3. *Solution of the compressible stability problem*

The 'quasi-parallel' compressible linear stability equations (2.36)–(2.40) may be written as a system of equations of the form

$$\left(\boldsymbol{A}\frac{\mathrm{d}^2}{\mathrm{d}y^2} + \boldsymbol{B}\frac{\mathrm{d}}{\mathrm{d}y} + \boldsymbol{C}\right)\boldsymbol{\phi} = 0, \tag{2.46}$$

where $\boldsymbol{\phi}$ is a five-element vector defined by $\{\hat{u}, \hat{v}, \hat{p}, \hat{T}, \hat{w}\}^{\mathrm{tr}}$ while $\boldsymbol{A}$ is a diagonal matrix and $\boldsymbol{B}$ and $\boldsymbol{C}$ are 5×5 matrices. Both the finite-difference and Chebyshev spectral methods for the solution of the above equation have been discussed by Malik (1990).

Here we use two different methods for the solution of the eigenvalue problem. First, we discretize (2.46) by a staggered finite-difference method and obtain the spatial eigenvalue α by using the QR algorithm. We use another method to purify the eigenvalues and obtain the eigenfunctions. To this end, we rewrite the second-order normal momentum equation as a first-order equation for pressure using the continuity equation. Thus, the above linear stability equations (2.46) may be transformed into a system of eight first-order equations:

$$\frac{\mathrm{d}\Psi_i}{\mathrm{d}y} - \sum_{j=1}^{8} a_{ij}\Psi_j = 0; \quad i = 1, 2, \ldots, 8, \tag{2.47}$$

where

$$\Psi_1 = \hat{u}, \quad \Psi_2 = \frac{\mathrm{d}\hat{u}}{\mathrm{d}y}, \quad \Psi_3 = \hat{v}, \quad \Psi_4 = \hat{p}, \quad \Psi_5 = \hat{T}, \quad \Psi_6 = \frac{\mathrm{d}\hat{T}}{\mathrm{d}y}, \quad \Psi_7 = \hat{w}, \quad \Psi_8 = \frac{\mathrm{d}\hat{w}}{\mathrm{d}y},$$

with corresponding boundary conditions

$$\Psi_1 = \Psi_3 = \Psi_5 = \Psi_7 = 0; \quad y = 0, \tag{2.48}$$

$$\Psi_1, \Psi_3, \Psi_5, \Psi_7 \to 0; \quad y \to \infty. \tag{2.49}$$

To solve (2.47)–(2.49), we use the compact difference scheme of Malik, Chuang & Hussaini (1982) which allows a fourth-order-accurate solution to be obtained on arbitrarily stretched grids. Both the eigenvalues and eigenfunctions are obtained by a third-order version of the Newton's method (see Malik 1990).

Equation (2.49) requires that the disturbance amplitude must be bounded at infinity. This condition may be satisfied in two ways. First, the disturbance amplitude can be simply set to zero at some large y. This works well for first- and second-mode 'subsonic' disturbances which decay quite fast. However, supersonic modes with $c_r < 1 - 1/M_e \cos\psi$ (see (3.4) below for ψ) and $-\alpha_i > 0$ appear when these Dirichlet boundary conditions are imposed. Alternatively, far-field boundary conditions, (2.49), can be imposed by obtaining the asymptotic solution of (2.46) in the uniform free stream. This is straightforward when curvature effects are ignored since in that case (2.46) reduces to an equation with constant coefficients. For the present case, however (2.46) does not reduce to an equation with constant coefficients owing to the dependence of m_{21} and m_{23} on y (see (2.42)) and therefore the free-stream conditions are derived by using WKBJ approximation with ϵ as the expansion parameter. The boundary conditions in this case can be imposed at some location outside the boundary layer. The stability results obtained this way agreed with those obtained by using zero perturbation conditions at a large y for the 'subsonic' modes referred to above. However, the supersonic modes were damped, at Reynolds numbers of the calculations, when asymptotic conditions were used.

3. Results and discussion

3.1. *Flow along a cylinder*

We first present results for flow along a cylinder, which is assumed to be hollow with sharp leading edges in order to avoid the complications introduced by leading-edge bluntness as discussed by Reshotko & Khan (1979) and Malik, Spall & Chang (1990). We choose a Mach number of 5 so that both the first- and second-mode disturbances can be studied at finite Reynolds numbers. Other flow parameters are the stagnation temperature, $T_0 = 540°R$, and unit Reynolds number, $u_e/\nu_e = 10^6$/ft. Adiabatic wall

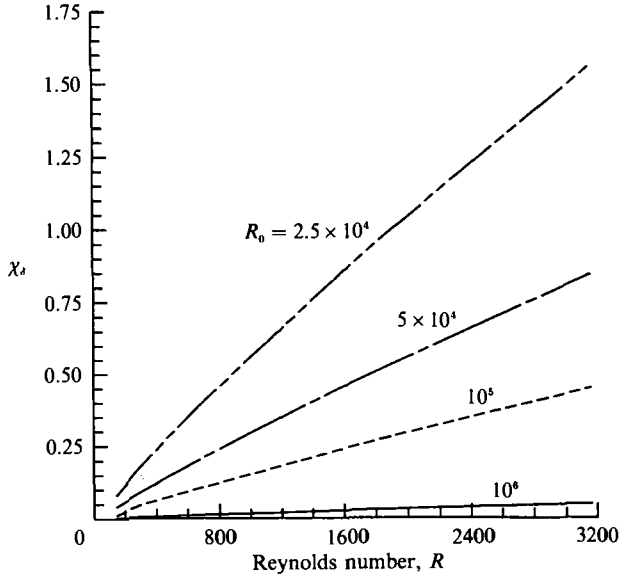

FIGURE 1. Transverse curvature parameter as a function of Reynolds number for cylinders of various radii and edge Mach number of 5. (The cylinder Reynolds number, $R_0 = u_e r_0/\nu_e$).

temperature conditions are assumed. Four different cylinder radii are considered; 0.025, 0.05, 0.1 and 1 ft which correspond to Reynolds numbers R_0 (based upon cylinder radius) of 2.5×10^4, 5×10^4, 10^5 and 10^6. R_0 can be used to characterize the effect of curvature. The basic flow was computed by solving boundary-layer equations (2.13)–(2.15) as discussed in §2.1. In accordance with (2.16*e*), we can define a curvature parameter χ_δ so that

$$\chi_\delta = \delta \cos\lambda / r_0, \tag{3.1}$$

where δ is the boundary-layer thickness based upon $u/u_e = 0.995$. We choose lengthscale ℓ (see (2.28)) as $\ell = (\nu_e x/u_e)^{\frac{1}{2}}$. The value of χ_δ for the four cylinders is plotted in figure 1 as a function of Reynolds number $R = (Re_x)^{\frac{1}{2}}$. The curvature parameter χ_δ is $O(1)$ for the smallest-radius cylinder, while $\chi_\delta \ll 1$ for the largest radius cylinder. So, the curvature effects will be expected to be negligible in the latter case.

At $R = 1414$ ($Re_x = 2 \times 10^6$), the mean velocity and temperature profiles for cylinders with $r_0 = 0.025$ ($\chi_\delta = 0.8106$) and 0.1 ft ($\chi_\delta = 0.2113$) are compared with the profiles for a flat-plate boundary layer ($\chi_\delta = 0$) in figure 2(*a*, *b*). These comparisons show that transverse curvature tends to decrease both the momentum and thermal boundary-layer thicknesses. We will note later that this thinning of the boundary layer will shift the second-mode instability to higher frequencies.

It is well known, according to Rayleigh's point-of-inflexion criterion, that velocity profiles which possess a point of inflexion are inviscidly unstable. Lees & Lin (1946) generalized this criterion to compressible flows. It has been found that the necessary and sufficient condition for the existence of a two-dimensional neutral subsonic wave ($1 - 1/M_e < c_r < 1 + 1/M_e$) is that at some point y_i in the boundary layer

$$\frac{\mathrm{d}}{\mathrm{d}y}\left(\rho \frac{\mathrm{d}U}{\mathrm{d}y}\right) = 0 \tag{3.2}$$

provided that $y_i > \bar{y}$, where $\bar{y}$ is the point at which $U = 1 - 1/M_e$. The phase velocity

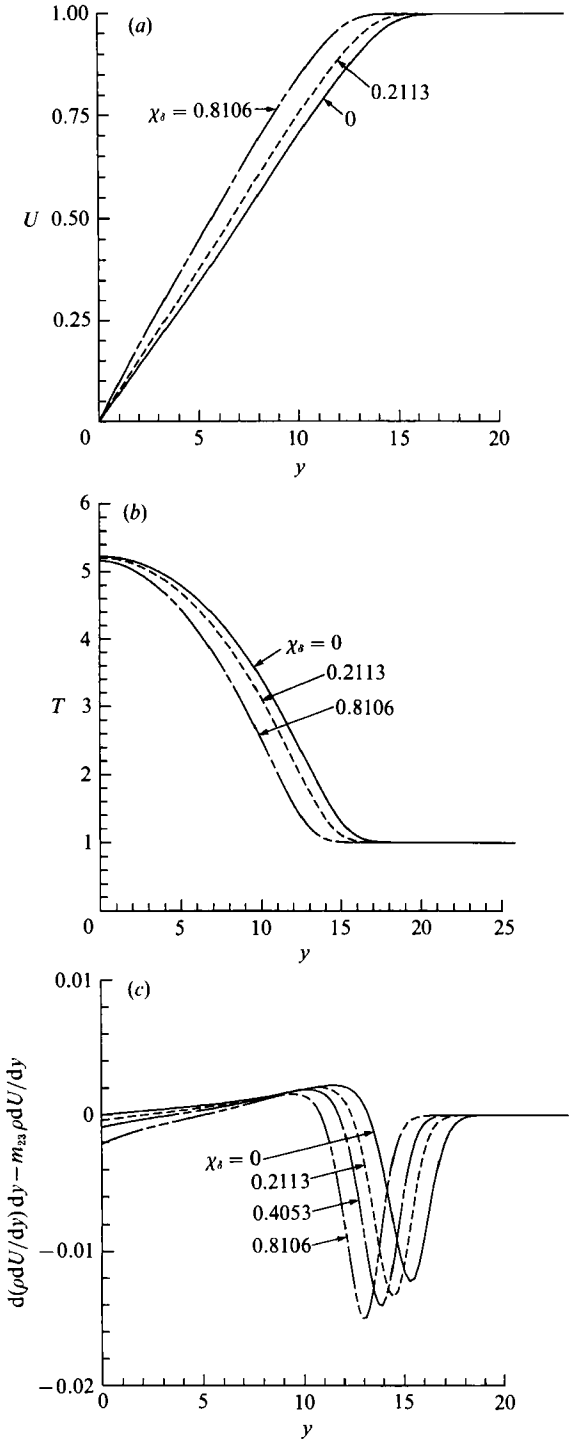

FIGURE 2. Comparison of mean flow profiles for Mach-5 adiabatic wall flow past a sharp flat plate and cylinders of different radii at a Reynolds number $R = 1414$: (*a*) velocity profiles, (*b*) temperatures profiles, (*c*) distribution of G_i (equation (3.3)).

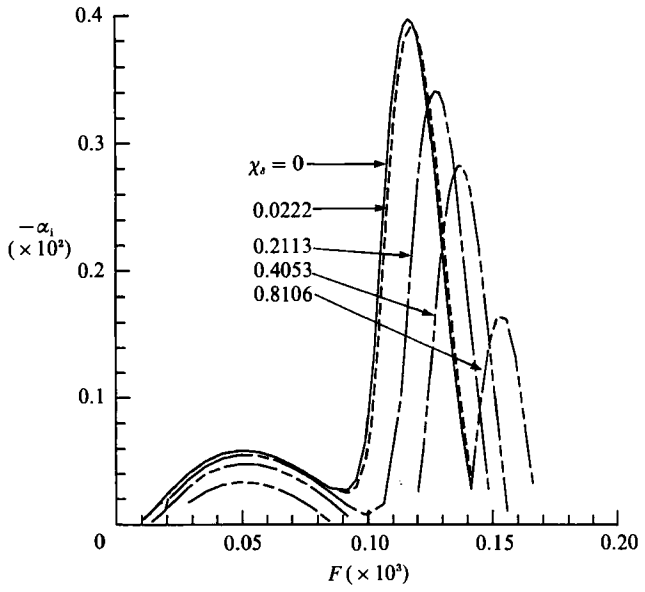

FIGURE 3. Comparison of spatial amplification rate for axisymmetric disturbances ($\beta = 0$) for a flat plate and cylinders with four different radii. Flow conditions are the same as in figure 2 ($M_e = 5$, $R = 1414$, adiabatic wall).

of the neutral wave is given as $c_r = U(y_i)$. The point y_i is known as the generalized inflexion point. The presence of the generalized inflexion point is also a sufficient condition for the existence of amplified waves. A compressible flat-plate (insulated wall) boundary layer contains one such inflexion point. By writing the compressible Rayleigh equation in cylindrical coordinates, and following the arguments used by Lees & Lin (1946), the generalized inflexion-point condition for axisymmetric flows can be derived as

$$G_i = \frac{\mathrm{d}}{\mathrm{d}y}\left(\rho\frac{\mathrm{d}U}{\mathrm{d}y}\right) - m_{23}\rho\frac{\mathrm{d}U}{\mathrm{d}y} = 0. \tag{3.3}$$

The quantity G_i for the flat plate ($\chi_\delta = 0$) and cylinders of three different radii is plotted in figure 2(*c*). While for the flat plate G_i has only one zero within the boundary layer, the cylinder boundary layer contains an additional zero near the wall. As χ_δ increases, this additional inflexion point moves away from the wall towards the outer inflexion point. However, the additional inflexion point remains below $y = \bar{y}$ for the present conditions. The two inflexion points are also known to exist in a flat-plate boundary layer with wall cooling and suction. With sufficient wall cooling the two inflexion points merge, and the boundary layer is free of them. Transverse curvature seems to have an effect on the mean boundary-layer profiles similar to that of cooling and suction, as also noted in the context of the boundary-layer thickness. It will be interesting to investigate how curvature affects the stability of axisymmetric flows. It is known that wall suction can be used to stabilize both first and second modes; however, wall cooling has a rather mixed effect: the first mode is stabilized while the second mode is made more unstable.

The results of stability calculations for $R = 1414$ are presented in figure 3 for axisymmetric disturbances ($\beta = 0$). The solid line is for a flat plate ($\chi_\delta = 0$). The curve for $\chi_\delta = 0$ shows a sharp peak in the growth rate $-\alpha_i$ at a non-dimensional frequency of $F = (\omega/R) = 0.000116$, corresponding to the second-mode instability. A

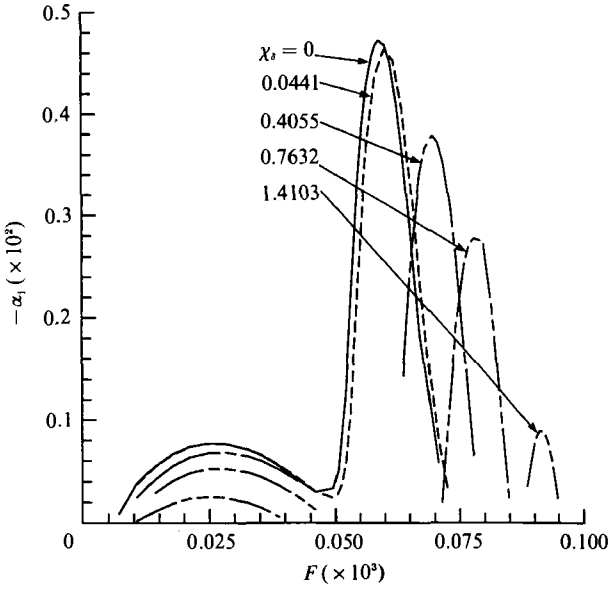

FIGURE 4. Same as in figure 3 except for $R = 2828$.

second, rather flat peak, with a much lower growth rate, exists at $F = 0.00005$, which is in the region of first-mode instability. As the curvature parameter χ_δ is increased we note several effects. The first is that the second-mode instability shifts to higher frequency. This effect is also found, for example, with wall suction. Both suction and transverse curvature tend to decrease the boundary-layer thickness, and since second-mode disturbance wavelength scales with boundary-layer thickness, the disturbance frequency increases. The second, and more important effect, is that the peak growth rate decreases as χ_δ increases; the peak growth is decreased by a factor of almost 2 when χ_δ is increased from 0 to 0.8. A similar effect was noted in the inviscid calculations of Duck (1990). The effect of transverse curvature on the lower, broader hump of axisymmetric disturbances in the first-mode region is also stabilizing. However, the peak disturbance frequency does not change but, if at all, shifts to slightly lower frequencies as evident in figure 4.

Figure 4 contains results for axisymmetric disturbances at $R = 2828$. Owing to an increasing boundary-layer thickness, χ_δ increases with Reynolds number (see figure 1). Thus, the stabilizing effect of curvature becomes more pronounced at higher Reynolds numbers. The peak second-mode growth rate at this Reynolds number decreases by a factor of 5 when χ_δ is increased from 0 to 1.4. A similar stabilizing trend is noted for the first-mode axisymmetric disturbances. The continued presence of the curvature effect at this higher Reynolds number shows that our results would not qualitatively change had non-parallel computations been performed.

It was noted in the discussion of figure 2(*a–c*) that the mean flow changes owing to transverse curvature. It may be interesting to see how much of the effect on the disturbance growth rate comes from change in the mean flow, and how much by the curvature terms in the stability equations. In order to study this we computed the mean flow for the cylinders, including transverse curvature, but solved the planar stability equations (ignoring the curvature effect). A significant effect was noted on the second-mode growth rate which indicates that the transverse curvature effect in the computation of the mean flow cannot be ignored.

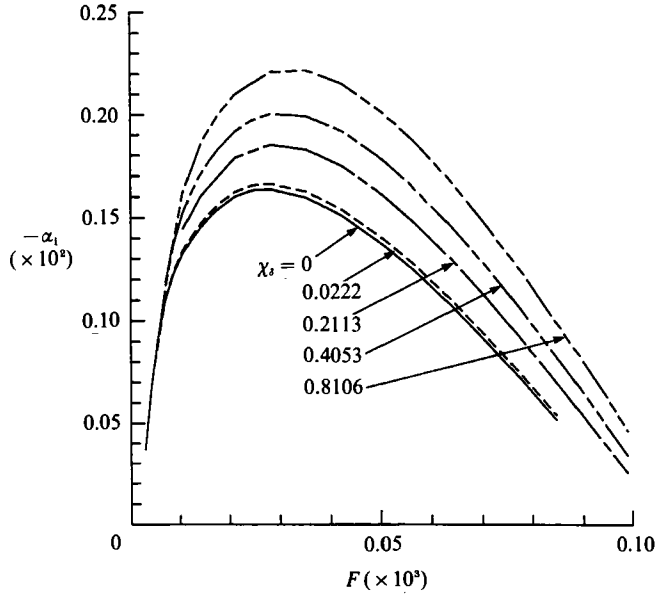

FIGURE 5. Comparison of spatial amplification rate for asymmetric (oblique, most amplified first mode) disturbances for a flat plate and cylinders with four different radii in Mach-5 flow ($R = 1414$).

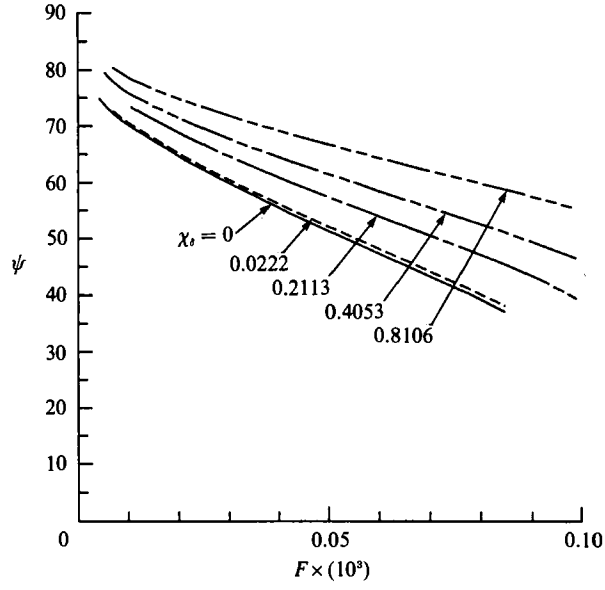

FIGURE 6. Distribution of wave angle for the most amplified disturbances computed in figure 5.

It is well known that first-mode disturbances are more amplified when oblique. It is, therefore, of interest to study the effect of transverse curvature on asymmetric disturbances. Such calculations are performed for disturbances which are most amplified, i.e. they satisfy the condition $d\alpha_1/d\beta = 0$. The growth rate curve thus generated will envelope the individual growth curves for fixed values of n (see (2.35*b*)). The results are presented in figure 5 for a Reynolds number of $R = 1414$. Contrary to the case of the axisymmetric disturbances, we find that asymmetric

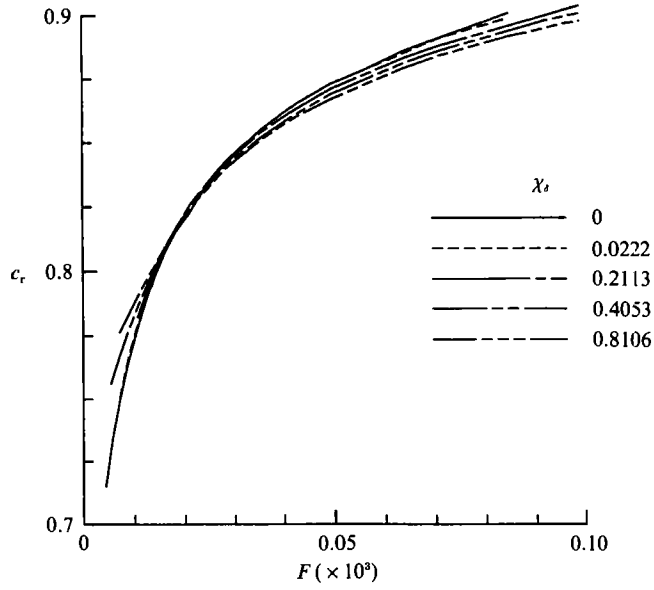

FIGURE 7. Distribution of phase velocity for the most amplified disturbances computed in figure 5.

disturbances are destabilized by transverse curvature. It may be noted in figure 5 that the peak growth rate increases by 40–50% when the curvature parameter is increased. The band of unstable frequencies also expands when curvature is increased. A similar trend was noted at a Reynolds number of 2828.

The disturbance wave angle ψ, where

$$\psi = \tan^{-1}(\beta/\alpha_r) \tag{3.4}$$

is plotted in figure 6 for the calculation at $R = 1414$. This shows that the first-mode instability waves that grow the fastest are inclined at relatively large angles with respect to the free stream, and that the angles increase with increasing curvature. The disturbance phase velocity c_r is given in figure 7. The phase velocity increases with frequency while the most amplified wave angle decreases with frequency; the largest wave angles being around 75–80° at the lowest frequencies computed here. Smith (1989) found that the most amplified wave orientation given by triple-deck theory agrees well with Mack's (1969) theory up to low supersonic Mach numbers. However, there appears to be a disagreement between the two theories as the Mach number is increased. At a Mach number of 5, for example, the most amplified wave angle given by the triple-deck theory is about 80°, as opposed to about 60° given by Mack's theory (compare figures 5 and 6 for $\chi_\delta = 0$). The disagreement may be due to the fact that the triple-deck structure is strictly valid for compressible flows near the lower branch where the phase velocity (see figure 7) is low enough so that the critical layer may be contained in the lower deck. At low frequencies, i.e. near the lower branch, the most amplified wave angle given by Mack's theory corresponds to that given by triple deck. It is known that, for incompressible Blasius flow, where both neutral branches describe viscous instability, the disturbance structure changes at higher frequencies, and is described by a multiple-deck structure (Bodonyi & Smith 1981) at the upper branch. For compressible Blasius flow at large Reynolds numbers, the upper-branch instability is of the inviscid Rayleigh type. Since the compressible

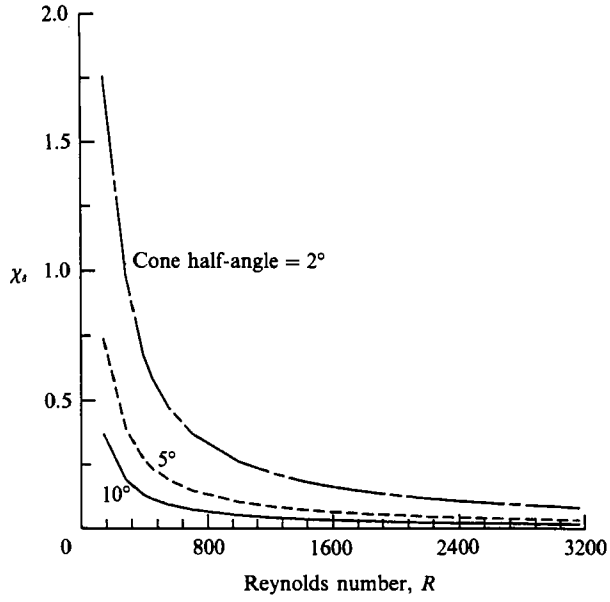

FIGURE 8. Transverse curvature parameter as a function of Reynolds number for three different sharp cones and edge Mach number of 5.

Rayleigh equation is a limiting form of the full viscous compressible linear equations, Mack's theory is capable of making the transition from TS instability at the lower branch (which triple deck describes) to Rayleigh instability at the upper branch. The same cannot be said about the triple-deck approach. In other words, triple-deck structure would break down much earlier for the compressible flow relative to the incompressible case when disturbance frequency is increased away from the lower branch. This is a plausible explanation of the differences at high Mach numbers between Mack's theory and Smith's theory, since the former had been experimentally validated by Kendall (1975) at Mach 4.5. For a flat plate in a Mach 4.5 stream, Kendall (1967) measured the disturbance phase velocity for an artificially generated $\psi = 55°$ wave. It was found that the phase velocity varied from about 0.7 to 0.9, which agrees with the quasi-parallel flow results such as those given in figure 7. Obviously, these observed high-phase-velocity disturbances, associated with the generalized inflexion point inviscid criterion, cannot be fitted in the lower deck of a triple-deck framework. It is only at lower Mach numbers, where viscous effects are much more important, that the results of Mack's theory and Smith's triple-deck theory would agree.

3.2. *Flow past a sharp cone*

We now investigate the stability of a more practical configuration; that of a sharp cone. The sharp-cone flow, in addition to having transverse curvature, also has a body divergence effect signified by the term $\mathrm{d}(\ln r_0)/\mathrm{d}x$ in (2.42*a*). We consider various cone angles and use a boundary-layer edge Mach number of 5, and the same wind tunnel temperature conditions as used for the cylinder. Though various cone angles imply that free-stream Mach number changes, it is sensible to fix the boundary-layer-edge Mach number in order to investigate curvature effects.

Here, three different cone half-angles (2°, 5°, 10°) are considered. The curvature parameter χ_δ for the three cones is plotted in figure 8. Since the cone radius increases faster than the boundary-layer thickness, the curvature parameter decreases both

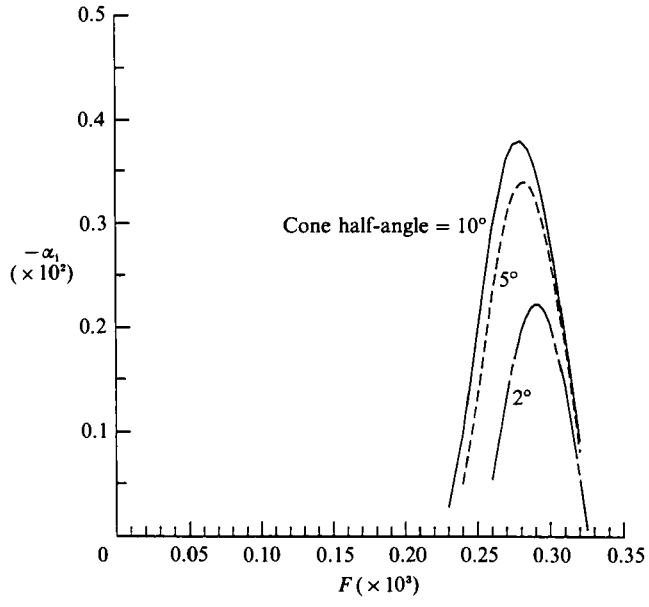

FIGURE 9. Comparison of spatial amplification rate for axisymmetric disturbances ($\beta = 0$) for 2°, 5° and 10° sharp cones at $R = 1000$. All three cones have the same edge Mach number and same unit Reynolds number.

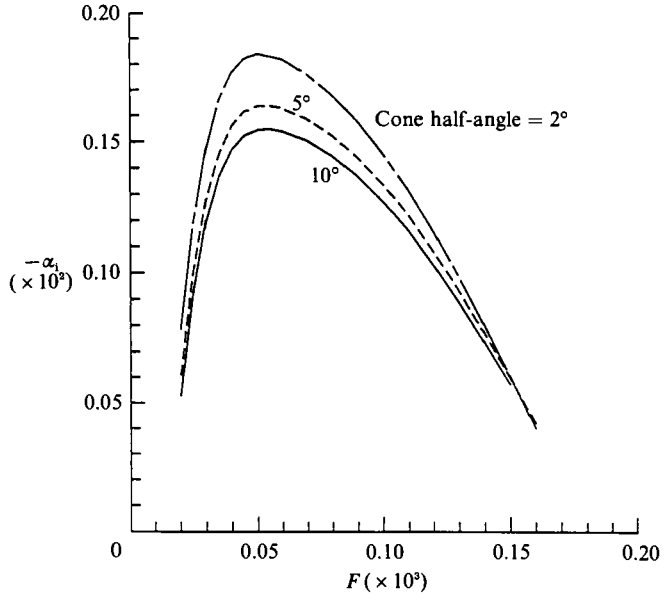

FIGURE 10. Comparison of spatial amplification rate for asymmetric (oblique first mode) disturbances for 2°, 5° and 10° sharp cones at $R = 1000$. Most-amplified disturbances ($d\alpha_i/d\beta = 0$) are computed.

with increasing Reynolds number, and with increasing cone angle. Accordingly, the effect of transverse curvature will decrease with increasing Reynolds number (it increased for a constant-radius cylinder owing to the thickening boundary layer) and with increasing cone angle.

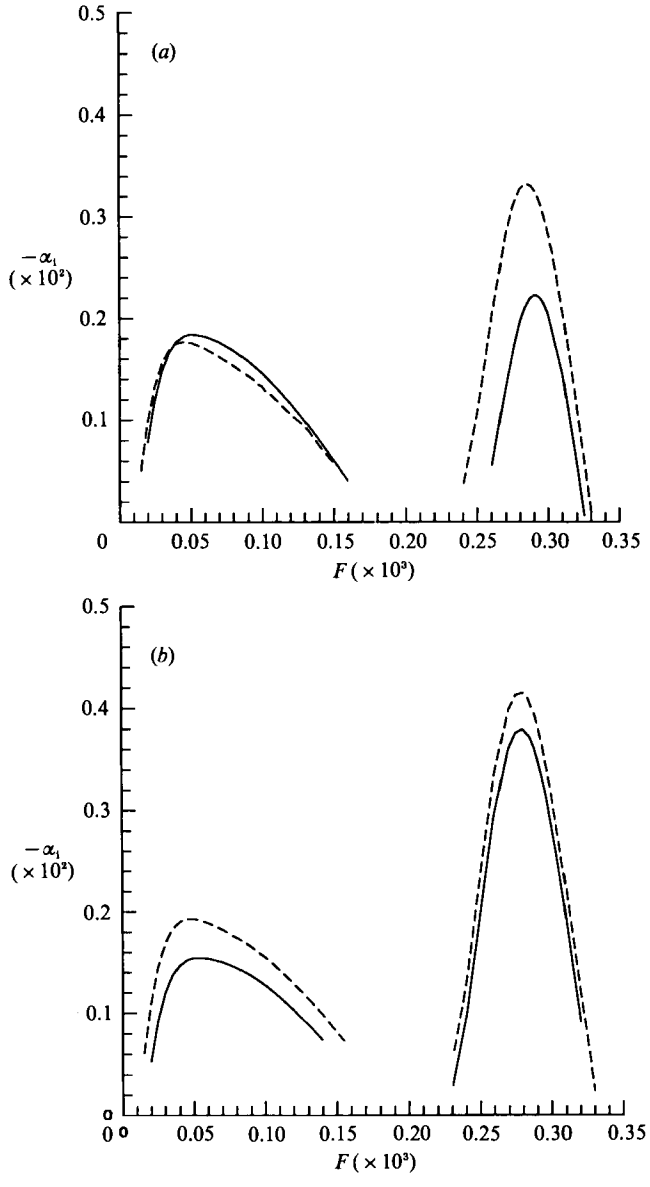

FIGURE 11. Comparison of first- and second-mode growth rates with the results of planar stability theory: (*a*) 2° cone, (*b*) 10° cone. ——, Present theory; – – – –, planar stability theory.

The stability results are presented at a Reynolds numbers of 1000 in figure 9, which shows the growth rates for axisymmetric disturbances for cone angles of 2°, 5° and 10° at a Reynolds number of 1000. The peak second-mode growth rate decreases as the cone angle decreases owing to the increasing effect of transverse curvature, as noted in the discussion of results presented for cylinders. Additional calculations for axisymmetric disturbances at $R = 2828$ showed an effect similar to that noted in figure 9, although the stabilization with decreasing cone angle lessened for the higher Reynolds number. This is due to the decrease in χ_δ with Reynolds number for a sharp cone. It should be pointed out that we have performed the above calculations for the three cones by fixing the boundary-layer-edge Mach number. However, if the free-

stream (ahead of the shock) Mach number is fixed, the corresponding boundary-layer-edge Mach numbers will be different for different cones (approximately 4.9 for 2° cone and 4.3 for 10° cone in a Mach 5 free stream).

We now consider asymmetric disturbances at $R = 1000$. The corresponding results are presented in figure 10. Since decreasing the cone angle implies higher transverse curvature, the peak growth rate increases when the cone angle is decreased owing to the destabilizing influence of transverse curvature on the asymmetric disturbances. The growth rates obtained by using the present theory are compared with the results of the planar stability equations in figure 11 for 2° and 10° cones. For the first oblique mode, the growth rates of the planar stability theory are higher for the 10° cone, and slightly lower for the 2° cone, and this may be attributed to the competing effects of transverse curvature and body divergence. With respect to the results obtained by using the planar stability equations, the effect of transverse curvature is destabilizing, and the effect of body divergence is stabilizing. The combined effect depends upon the cone angle and may be stabilizing or destabilizing. The second-mode growth rates, using the present theory, are always lower than the planar stability results since both the transverse curvature and body divergence exert a stabilizing influence. In any case, the effect diminishes with Reynolds number.

4. Conclusions

We have studied linear stability of supersonic flow past a series of cylinders and sharp cones with various nose angles in order to delineate the effects of transverse curvature and body divergence. We find that transverse curvature helps to stabilize axisymmetric first- and second-mode disturbances while it makes asymmetric disturbances (oblique first-mode waves) more unstable. These effects progressively become pronounced when the curvature parameter χ_δ (see (3.1)) is increased to $O(1)$ values and the results of planar stability theory are recovered when $\chi_\delta \to 0$. We note that for some intermediate values of Mach number, the dominant instability could shift from the second mode to the first mode because curvature has a stabilizing and destabilizing effect, respectively, on these modes. A similar shift from first to second mode takes place owing to wall cooling which stabilizes the first mode and destabilizes the second mode.

The results obtained for sharp cones show that transverse curvature effects are important near the nose (small Reynolds numbers) with small nose angles, and the effect gradually disappears with increasing Reynolds number or increasing cone angle. On the other hand, the body divergence effect increases with increasing cone angle and is stabilizing for both the axisymmetric and asymmetric disturbances. It is hoped that using the present theory for axisymmetric flows will resolve some of the discrepancies between the sharp-cone experiments and the planar stability theory results. However, it should be pointed out that we have used the quasi-parallel approximation in this study, and it remains to be seen whether the qualitative nature of the effect of curvature will change when this approximation is relaxed.

This work was partly sponsored by NASA Langley Research Center under Contract NAS1-18240.

REFERENCES

BECKWITH, I. E., CREEL, T. R., CHEN, F.-J. & KENDALL, J. M. 1983 *NASA TP*-2180.

BODONYI, R. J. & SMITH, F. T. 1981 *Proc. R. Soc. Lond.* A **375**, 65.

CHANG, C.-L., MALIK, M. R. & HUSSAINI, M. Y. 1990 *AIAA Paper* 90-1448.

CHEN, F.-J., MALIK, M. R. & BECKWITH, I. E. 1989 *AIAA J.* **27**, 687.

COWLEY, S. & HALL, P. 1990 *J. Fluid Mech.* **214**, 17.

DEMETRIADES, A. 1974 *AIAA Paper* 74-535.

DUCK, P. W. 1990 *J. Fluid Mech.* **214**, 611.

DUCK, P. W. & HALL, P. 1989 *Q.J. Mech. Appl. Maths* **42**, 115.

EL-HADY, N. M. 1981 *NASA CR*-3474.

GAPANOV, S. A. 1981 *Proc. Eighth Canadian Cong. of Appl. Mech.*, p. 673.

GASPERAS, G. 1987 *AIAA Paper* 87-0494.

GASTER, M. 1974 *J. Fluid Mech.* **66**, 465.

HARRIS, J. E. & BLANCHARD, D. K. 1982 *NASA TM*-83207.

HAYES, W. D. & PROBSTEIN, R. F. 1959 *Hypersonic Flow Theory*. Academic.

KENDALL, J. M. 1967 *Aerospace Corp. Rep.* BSD-TR-67-213, vol. II.

KENDALL, J. M. 1975 *AIAA J.* **13**, 290.

LEES, L. & LIN, C. C. 1946 *NACA TN* 1115.

LEES, L. & RESHOTKO, E. 1962 *J. Fluid Mech.* **12**, 555.

MACK, L. M. 1969 *Jet Propulsion Lab Rep.* 900-277.

MACK, L. M. 1984 *AGARD Rep.* 709.

MACK, L. M. 1987 *AIAA Paper* 87-1413.

MALIK, M. R. 1984 *Energy Resources Tech. Conf. ASME, FED*-Vol. 11, p. 139.

MALIK, M. R. 1989*a* *AIAA J.* **27**, 1487.

MALIK, M. R. 1989*b* In *Laminar–Turbulent Transition*, p. 251. Springer.

MALIK, M. R. 1990 *J. Comput. Phys.* **86**, 376.

MALIK, M. R., CHUANG, S. & HUSSAINI, M. Y. 1982 *Z. Angew. Math. Phys.* **33**, 189.

MALIK, M. R. & POLL, D. I. A. 1985 *AIAA J.* **23**, 1362.

MALIK, M. R., SPALL, R. E. & CHANG, C.-L. 1990 *AIAA Paper* 90-0112.

MALIK, M. R., WILKINSON, S. P. & ORSZAG, S. A. 1981 *AIAA J.* **19**, 1131.

MORKOVIN, M. V. 1969 *AFFDL*-TR-68-149.

PATE, S. R. 1971 *AIAA J.* **9**, 1082.

PATE, S. R. & SCHEULER, C. J. 1969 *AIAA J.* **7**, 450.

PETROV, G. V. 1985 In *Laminar-Turbulent Transition*, p. 487. Springer.

PROBSTEIN, R. F. & ELLIOTT, D. 1956 *J. Aeronaut. Sci.* **23**, 208.

RESHOTKO, E. & KHAN, M. M. S. 1979 In *Laminar-Turbulent Transition*, p. 186. Springer.

SMITH, F. T. 1989 *J. Fluid Mech.* **198**, 127.

STETSON, K. F., THOMPSON, E. R., DONALDSON, J. C. & SILER, L. G. 1983 *AIAA Paper* 83-1761.

STEWARTSON, K. 1964 *Theory of Laminar Boundary Layers in Compressible Fluids*. Oxford University Press.

TOLLMIEN, W. 1929 *Nachr. Ges. Wiss. Göttingen, Math.-Phys. Klasse*, p. 21.